SAND2021-12979C

Experimental and Computational Investigation of Nonlinear Dynamics of a Simplified Bearing-and-Shaft Assembly

Nathaniel N. Goldberg[1], Sarah Demsky[2], Abdelrahman A. Youssef[3], Steven P. Carter[4], Deborah Fowler[4], Nathan Jackson[5], Robert J. Kuether[4], Andrew Steyer[4]

[1]Department of Mechanical Engineering
University of California, Berkeley

[2]Department of Aeronautics and Astronautics
Massachusetts Institute of Technology

[3]Department of Mechanical Engineering
Texas A&M University

[4]Engineering Sciences Center
Sandia National Laboratories

[5]Department of Mechanical Engineering
University of New Mexico

ABSTRACT

Mechanical assemblies often have significant nonlinearities stemming from impacts between parts, limiting the applicability of linear modal analysis. One motivating example in mechanical engineering is a bearing-and-shaft assembly in which the contact nonlinearity is due to small radial clearances in the roller bearings. Impacts can cause the rigid-body modes of individual parts to couple with higher frequency elastic modes in an intricate, nonlinear manner, potentially leading to dynamic amplification at frequencies significantly above or below those predicted by modal analysis of the linearized system. A thorough understanding of the resonant behavior is especially important when the assembly is subjected to broadband excitations such as shock loads, which can excite the system's modes to different energy levels. This work identifies the nonlinear resonances stemming from the low frequency pseudo-rigid-body modes in a simplified representation of a bearing-and-shaft assembly and explores how these modes evolve into elastic modes of the shaft at higher energies. The ensuing spectra of the transient ringdown from a shock-type load are then analyzed in the context of the nonlinear normal modes of the system.

Keywords: *nonlinear dynamics, contact nonlinearity, nonlinear normal modes, time-frequency analysis*

1. Introduction

Engineered assemblies are often required to perform their design function in a wide range of mechanical environments. Two main areas of focus within the mechanical environment space are low-amplitude, long-duration random vibration and high-amplitude, short-duration mechanical shock. Low-level vibration is

traditionally analyzed using linear structural dynamics techniques (i.e. modal analysis) which essentially utilize a small number of modal solutions to reconstruct the dynamic response using the principal of superposition [1]. One of the primary objectives of modal analysis is to determine if a structure's resonant response could cause dynamic amplification of specific frequency content in the service environment, leading to significantly higher deformations and stresses than would be predicted by a quasi-static structural analysis. Linear modal analysis is appropriate for structures that respond approximately linearly, as is the case in some low-amplitude vibration environments.

Conversely, mechanical shocks are high-amplitude events and often can cause structures to respond in a strongly nonlinear manner, necessitating the use of solid mechanics models to accurately capture the relevant physics, such as contact-impacts, large deformations, and plasticity. Although solid mechanics models inherently capture a structure's resonant behavior in their solution, a single transient simulation is insufficient to understand the system's dynamics and response with varying excitation frequency/amplitude as linear modal analysis typically does.

This study stems from electromechanical systems and components whose sources of nonlinearity primarily come from friction and contact between piece parts and plastic deformations due to large strains. These physics limit or invalidate the assumptions needed to apply linear modal analysis techniques. Severe mechanical shocks can produce significant plastic deformation that alters the material stiffness and energy dissipation. Conversely, contact impacts often do not lead to global plastic deformation but still significantly alter the stiffness of the individual piece parts depending on the time-varying contact status (open, closed, slipping).

Examples of typical piece parts that generate contact during nearly any mechanical environment are bearings and backlash in gears. Such piece parts are exceedingly common in electromechanical components and present significant challenges to understand their resonant behavior and response. Many studies have investigated the consequence of vibro-impact for the response to shock-type loading. One recent study by Gzal et al. [2] investigates the occurrence of intermodal targeted energy transfer of a civil structure with inelastic Hertzian vibro-impacts, which causes energy transfer of low-frequency vibration modes to higher-frequency ones.

Linear modal analysis of electromechanical mechanisms can, in theory, be formulated by linearizing all the contact interfaces and deciding whether interfaces are either fully tied (i.e. constraints in normal and tangential directions), slipped (i.e. normal tied constraints only) or free. The paper by Herrera et al. [3] discuss how a nonlinear system will behave linearly in the extreme limits of the response but respond nonlinearly within these limits. In certain designs and excitation levels, a linearized analysis may adequately capture all the relevant modes of vibration that could dynamically amplify in the service environment. Ideally the chosen modeling approach would capture the lowest frequency elastic modes of the structure, which are usually responsible for generating the largest stresses in critical piece parts.

Experience with high-fidelity finite element modeling of complex electromechanical assemblies with bearings and gears suggest that this is most often not the case. Contact impacts can cause the elastic modes of individual piece parts to couple with rigid body modes in a very complex, non-linear manner, ultimately leading to dynamic amplification at frequencies significantly below those predicted from a linearized modal analysis with tied constraints. This could lead to an inaccurate technical basis to accept a design of a structure based on a linear analysis. For example, one could predict that all sources of dynamic (elastic) amplification are of sufficiently high frequency outside the frequency range of the relevant service environments, when in fact non-linear coupling due to contact impacts introduces resonant frequencies into the range of the service environment's frequency content.

This research investigates the non-linear coupling associated with contact in bearings in electromechanical components by studying an idealized system designed to imitate the important physics. In this study, numerical experiments are conducted to understand how contact impacts lead to non-linear coupling between elastic and rigid body modes using undamped nonlinear normal mode theory [4] and time-frequency analysis methods [5] to analyze the spectral content of a transient ringdown response to shock-type loads. The evolution of rigid body modes into elastic modes can introduce significant stresses at lower resonant frequencies than predicted by the linearized modes of the system.

The paper is organized as follows. Section 2 provides a brief overview of nonlinear normal mode theory and the time-frequency analysis used to investigate the dynamics of the system. Section 3 presents the simplified discrete model and the virtual experiments conducted to demonstrate the evolution of the dynamics from elastic to pseudo-rigid body modes during transient ringdown. The spectra are compared with the nonlinear normal modes of the system to correlate the responses Section 4 details some preliminary experiments and high-fidelity finite element modeling of an experimental apparatus designed to replicate contact nonlinearity in a shaft supported by two bearing on each end. Conclusions are made lastly in Section 5.

2. Theoretical Development

2.1 Nonlinear Normal Modes

In this study, the undamped nonlinear normal modes of the system are of interest to understand the resonant behavior of the structure in the presence of small gap clearances, leading to nonlinear contact forces. The definition of the NNM adopted here is based on that of Kerschen and Vakakis [4], such that an NNM motion is a not necessarily synchronous periodic response of the nonlinear equations of motion. For a conservative mechanical system,

$$\mathbf{M}\ddot{\mathbf{x}} + \mathbf{K}\mathbf{x} + \mathbf{f}_{nl}(\mathbf{x}) = 0 \tag{1}$$

a periodic orbit must satisfy the condition $\mathbf{x}(t) = \mathbf{x}(t+T)$ for all t with a minimum period T. Several numerical methods are available to calculate the NNMs from a nonlinear system; in this study the harmonic balance (HB) method is utilized to calculate a branch of periodic solutions stemming from the linearized modes at low energy.

The HB method is a Fourier-Galerkin mathematical technique to solve for periodic solutions for nonlinear systems [6]. The periodic motion is approximated with a finite Fourier series as,

$$\mathbf{x}(t) = \frac{\mathbf{c}_0^x}{\sqrt{2}} + \sum_{k=1}^{N_h}\left[\mathbf{s}_k^x \sin(k\omega t) + \mathbf{c}_k^x \cos(k\omega t)\right] \tag{2}$$

The nonlinear restoring force can similarly be expressed as,

$$\mathbf{f}_{nl}(\mathbf{x}) = \frac{\mathbf{c}_0^f}{\sqrt{2}} + \sum_{k=1}^{N_h}\left[\mathbf{s}_k^f \sin(k\omega t) + \mathbf{c}_k^f \cos(k\omega t)\right] \tag{3}$$

Taking the time derivatives of the displacement field, substituting Eqns. (2) and (3) into Eq. (1), and performing a Galerkin projection onto the Fourier basis results in the algebraic system in the frequency-domain,

$$\mathbf{A}(\omega)\mathbf{z} + \mathbf{b}(\mathbf{z}) = \mathbf{0} \tag{4}$$

where $\mathbf{z}$ is the collection of unknown Fourier coefficients in Eq. (2), ω is the unknown fundamental frequency, $\mathbf{A}(\omega)$ is the linear dynamic stiffness matrix, and $\mathbf{b}(\mathbf{z})$ is the nonlinear restoring force calculated with the alternating frequency/time method [7].

The HB discretization in Eq. (4) is combined with an pseudo-arclength continuation scheme [8] to trace the branch of solutions, resulting in the NNM curves describing the change of resonance condition in the presence of nonlinear internal forces.

2.2 Time-Frequency Analysis

The system response to an external load and/or initial condition can be described by the damped equations of motion,

$$\mathbf{M}\ddot{\mathbf{x}} + \mathbf{C}\dot{\mathbf{x}} + \mathbf{K}\mathbf{x} + \mathbf{f}_{nl}(\mathbf{x}) = \mathbf{f}_{ext}(t) \tag{5}$$

$$\mathbf{x}(t=0) = \mathbf{x}_0$$

$$\dot{\mathbf{x}}(t=0) = \mathbf{v}_0$$

A shock-type loading can be applied either as an initial velocity at specific degrees-of-freedom, or as an external time-varying force applied over a short period. The resulting ringdown response can be computed for Eq. (5) using various time-marching schemes.

A time-frequency analysis of the ringdown response provides insight into the instantaneous spectral content of the response as the energy decays due to non-conservative forces. In this study, the short-time Fourier transform (STFT) is utilized to post-process the ringdown data for a single response location, denoted as $x(t)$. The STFT algorithm performs a fast Fourier transform (FFT) on a segment of data with an appropriate window applied over the sample and repeated along the entire time series by sliding the window along the time axis. Assuming the signal is stationary within each sample, the resulting spectra illustrates the instantaneous frequency content and how it evolves over time.

Assuming the signal, $x(t)$, is sampled at N evenly spaced points in time, the discrete samples from the ringdown are $x_0, x_1, \ldots, x_{N-1}$ where $x_n = x\left(\frac{nT}{N}\right)$ and T is the period of the response. An appropriate window function, denoted as $w(t-\tau)$, moves along the time axis at discrete time shifts, $\tau = \frac{mT_w}{N}$, with a shorter period than the measurement period, i.e. $T_w \ll T$. The time point m controls the center time of the window, allowing a FFT to be computed over different segments of the signal and approximate the instantaneous frequency content over each segment.

In this study, a Hanning window was used on each segment of the sampled data. The STFT results are displayed using a spectrogram to visualize the evolution of the frequency content of the transient ringdown as energy dissipates from the system.

3. Numerical Results: Simplified Discrete Model

Here we consider a model that reflects the essential in-plane dynamics of the experimental apparatus to be introduced in Section 4. The model, illustrated in Fig. 1, consists of three masses connected by rigid links. The outer masses m_1 and m_3 are suspended by pairs of soft springs with stiffness k_s, while the inner mass m_2 is coincident with a torsional spring with stiffness κ that emulates the bending stiffness of the shaft. The angular displacement in the spring is assumed to be small so that only vertical displacements of the masses are permitted. Such an arrangement results in three linear modes of vibration: a symmetric (translational) pseudo-rigid body mode, an antisymmetric (rotational) pseudo-rigid body mode, and a bending mode. When the absolute displacement of either outer mass is greater than the gap g, gap springs of stiffness k_g become active.

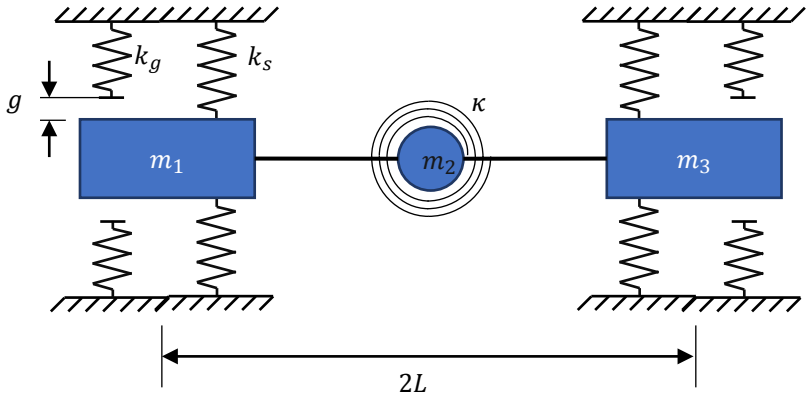

Figure 1. Discrete model of the planar dynamics of a simplified bearing-and-shaft assembly.

The equations of motion of the model can be readily obtained via Lagrange's method. The kinetic energy reads

$$T = \frac{1}{2}m_1\dot{x}_1^2 + \frac{1}{2}m_2\dot{x}_2^2 + \frac{1}{2}m_3\dot{x}_3^2 \tag{6}$$

and, under the assumption of small displacements, the potential energy is

$$U = k_s x_1^2 + \frac{\kappa}{2L^2}(x_1 - 2x_2 + x_3)^2 + k_s x_3^2 + U_g(x_1) + U_g(x_3) \tag{7}$$

where

$$U_g(x) = \begin{cases} \frac{1}{2}k_g(x-g)^2, x > g \\ 0, \ -g \le x \le g \\ \frac{1}{2}k_g(x+g)^2, x < -g \end{cases} \tag{8}$$

In view of the above expressions for the kinetic and potential energies, the equations of motion are

$$\begin{bmatrix} m_1 & 0 & 0 \\ 0 & m_2 & 0 \\ 0 & 0 & m_3 \end{bmatrix} \begin{bmatrix} \ddot{x}_1 \\ \ddot{x}_2 \\ \ddot{x}_3 \end{bmatrix} + \begin{bmatrix} 2k_s + \kappa/L^2 & -2\kappa/L^2 & \kappa/L^2 \\ -2\kappa/L^2 & 4\kappa/L^2 & -2\kappa/L^2 \\ \kappa/L^2 & -2\kappa/L^2 & 2k_s + \kappa/L^2 \end{bmatrix} \begin{bmatrix} x_1 \\ x_2 \\ x_3 \end{bmatrix} + \begin{bmatrix} f(x_1) \\ 0 \\ f(x_2) \end{bmatrix} = \begin{bmatrix} 0 \\ 0 \\ 0 \end{bmatrix} \tag{9}$$

where

$$f(x) = \begin{cases} k_g(x-g), x > g \\ 0, \ -g \le x \le g \\ k_g(x+g), x < -g \end{cases} \tag{10}$$

For the purposes of studying the ringdown response of Eq. (9), a proportional, diagonal damping matrix $c\boldsymbol{I}$ is added to the left-hand side, c being a small parameter and $\boldsymbol{I}$ the 3x3 identity. The damping is ignored for the purpose of studying nonlinear normal modes but is included in the transient simulations. Table 1 shows the parameter values used throughout this paper.

Table 1. Parameter values for the model illustrated in Figure 1.

Description	Symbol	Value
Suspension spring stiffness	k_s	8.03e3 N/m
Torsional spring stiffness	κ	79161 N m/rad
Gap spring stiffness	k_g	3.502e7 N/m
Half-length	L	0.1614 m
Gap	g	2.54e-4 m
Left mass	m_1	0.629 kg
Middle mass	m_2	1.258 kg
Right mass	m_3	0.629 kg
Damping coefficient	c	4 N s/m

3.1 Nonlinear Normal Modes

The nonlinear normal modes of the system in Eq. (9) are computed using harmonic balance with a pseudo-arclength continuation scheme, as described in Section 2.1. Note that each curve is computed with only a single harmonic to avoid excessive computations of the many internal resonances occurring along NNM 1. The frequency-energy plots (FEPs) are plotted in Fig. 2. Each NNM begins at the linearized natural frequency at low energy, resulting in a straight curve since the contact nonlinearity is not engaged in these energy ranges. The black dashed lines correspond to the linearized natural frequencies, f_n, when the gap springs are in an open state.

Each NNM reaches a critical energy level at which the gap spring engages, causing the resonant frequency to increase, or stiffen. Note that this energy level can be controlled by the gap distance. As the energy of the periodic motion increases, the frequency continues to increase until saturating towards an upper frequency limit. These limiting values, $f_{n,t}$, correspond to the linearized state when the gap springs are closed and included in the tangent stiffness matrix. The red dashed curves correspond to the linearized frequencies for an assumed closed gap.

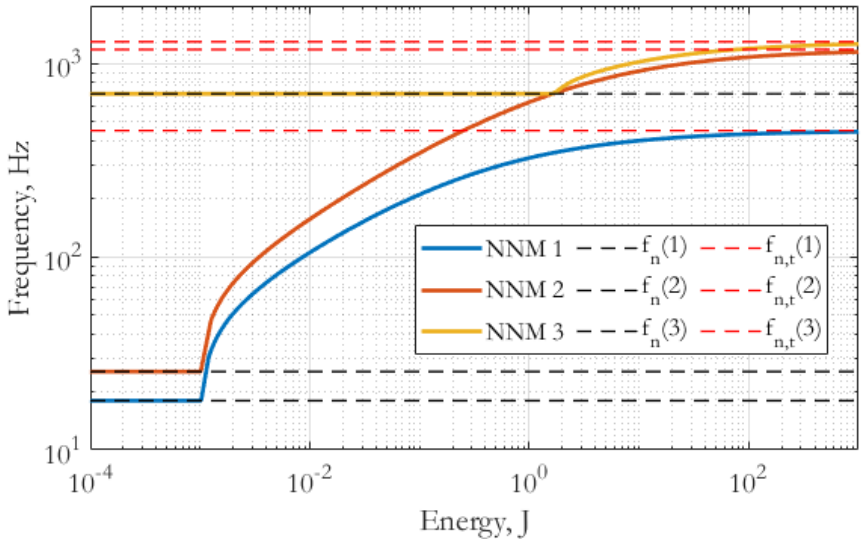

Figure 2. Frequency-energy plots of the three undamped NNMs for the simplified discrete model.

The NNMs of the system reveal several interesting characteristics of the dynamics. Depending on how one would choose to linearize the system (e.g. either gap open or closed), the resulting linear natural frequencies would significantly differ. In the context of bearing-and-shaft assemblies, it may be difficult to know which linearized state to assume for a given system – (i.e. does a small clearance gap exist between the housing and the bearings/races?). Assuming an open gap case would result in a shaft that has purely rigid body motion, which would often be an undesirable approach to modeling a shaft supported by bearings. On the contrary, assuming a closed gap state to linearize the system would result in resonant behavior described by the upper frequency limit of the NNMs. This may not be a conservative estimate as the true system (i.e. nonlinear system with contact/impact) may exhibit resonant behavior at intermediate frequencies between the two limits. The NNMs reveal the energy ranges in which these limiting, linearized cases may be appropriate, but also provide insight into the energy ranges in which a linearized model is inadequate. As will be shown in Section 3.2, the dynamics of the system during transient ringdown show a range of frequency content consistent with the NNMs of the system and the energy input into the system.

In addition to the NNM solutions obtained using the HB approach, an analytical derivation for NNM 2 is provided to validate the numerical results. NNM 2 is an antisymmetric mode, meaning that $x_1 = -x_3$ and $x_2 = 0$. Assuming $m_1 = m_3$ (as is the case for the values in Table 1), Eq. (9) then reduces to a single piecewise linear oscillator,

$$m_1\ddot{x}_1 + 2k_s x_1 + f(x_1) = 0 \tag{11}$$

For $|x_1| < g$, the angular natural frequency is simply $\omega_0 = \sqrt{2k_s/m_1}$. Because Eq. (11) is piecewise linear, it can be solved separately in closed form for the cases $x_1 > g$, $x_1 < -g$, and $|x_1| < g$, after which the solutions can be stitched together by ensuring continuity of x_1 and $\dot{x}_1$. The availability of analytical solutions makes it possible to develop an exact expression for the relationship between frequency and energy in NNM 2. To do this, consider (without loss of generality) the initial conditions $x_1(0) = x_0 > g$ and $\dot{x}_1(0) = 0$. Introducing the dimensionless

parameters $\chi_0 = x_0/g$ and $K = k_g/(2k_s)$, it can be shown that the time spent in the regime $|x_1| > g$ over the course of one period is

$$T_g(x_0) = \frac{4}{\omega}\cos^{-1}\frac{1}{\chi_0(1+K)-K} \tag{12}$$

while the amount of time spent in $|x_1| < g$ is

$$T_s(x_0) = \frac{4}{\omega_0}\cot^{-1}\frac{\chi_0(1+K)-K}{\sqrt{1+K}} \tag{13}$$

and thus the (angular) frequency-amplitude relationship is,

$$\omega(x_0) = \begin{cases} 2\pi\left[T_g(x_0) + T_s(x_0)\right]^{-1} & x_0 > g \\ \omega_0 & x_0 < g \end{cases} \tag{14}$$

Conservation of the total mechanical energy implies that $E = 2k_s x_0^2 + k_g(x_0 - g)^2$, an expression that can be inverted to give the amplitude of oscillations as a function of the energy: $x_0 = x_0(E)$. Then, the exact frequency-energy relationship for NNM 2 follows as $\hat{\omega}(E) = \omega(x_0(E))$.

It is important to emphasize that the harmonic balance method discussed previously produces frequency-energy relationships for each NNM that are numerical and inexact due to the approximation of representing the periodic solution with a finite Fourier series. In what follows, we denote them by $\breve{\omega}_1(E)$, $\breve{\omega}_2(E)$, and $\breve{\omega}_3(E)$, keeping in mind that we use $\hat{\omega}(E)$ to denote the exact relationship for NNM 2 derived above. Also worth noting is that $\hat{\omega}(E) \to \sqrt{(2k_s + k_g)/m_1}$ as $E \to \infty$, the correct closed-gap limit.

3.2 Transient Ringdown Analysis

If the system is initiated from rest at some point along one of the frequency-energy curves, then it will remain at that point for all time. However, if light viscous damping is included, then the system will approximately obey the frequency-energy relationship as it "rings down" from high energy to low energy due to the invariance property of the mode. In the case of the simplified discrete system, the response may start from the closed-gap natural frequency and transition to the open-gap natural frequency. Once enough energy has been dissipated such that impacts with the gap springs cease, the system regains linearity and further oscillations occur at the (damped) open-gap frequency, independent of amplitude. In the case of NNM 2, the energy at which this transition occurs is $2k_s g^2$.

To demonstrate the utility of both the analytical and harmonic balance-derived frequency-energy relationships in characterizing the transient ringdown response, we compute numerically the antisymmetric motion due to the initial conditions $x_1(0) = 100g$ and $\dot{x}_1(0) = 0$. Figure 3 (left) shows a spectrogram of $x_1(t)$ with $\hat{\omega}(E(t))/(2\pi)$ and $\breve{\omega}_1(E(t))/(2\pi)$ overlaid. Clearly, both the analytical and harmonic balance predictions agree well with the transient numerical results and the ringdown follows the frequency of the underlying NNM. Additional harmonics included in the HB computations would improve the accuracy and agreement with the analytical data.

As an example, consider the initial conditions $\boldsymbol{x}(0) = [0\ 0\ 0]^T$ and $\dot{\boldsymbol{x}}(0) = [0\ 0\ 200\ \mathrm{m/s}]^\mathrm{T}$, which are meant to model an impulse-like loading on the system. A spectrogram of $x_1(t)$ is shown in Figure 3 (right) with $\breve{\omega}_1(E(t))$, $\breve{\omega}_2(E(t))$, and $\breve{\omega}_3(E(t))$ superimposed. The spectrograms for $x_2(t)$ and $x_3(t)$ are similar. Although the spectrogram shows some complicated structures likely related to numerical idiosyncrasies and interactions between modes, the primary frequency content indeed appears along the three NNM curves.

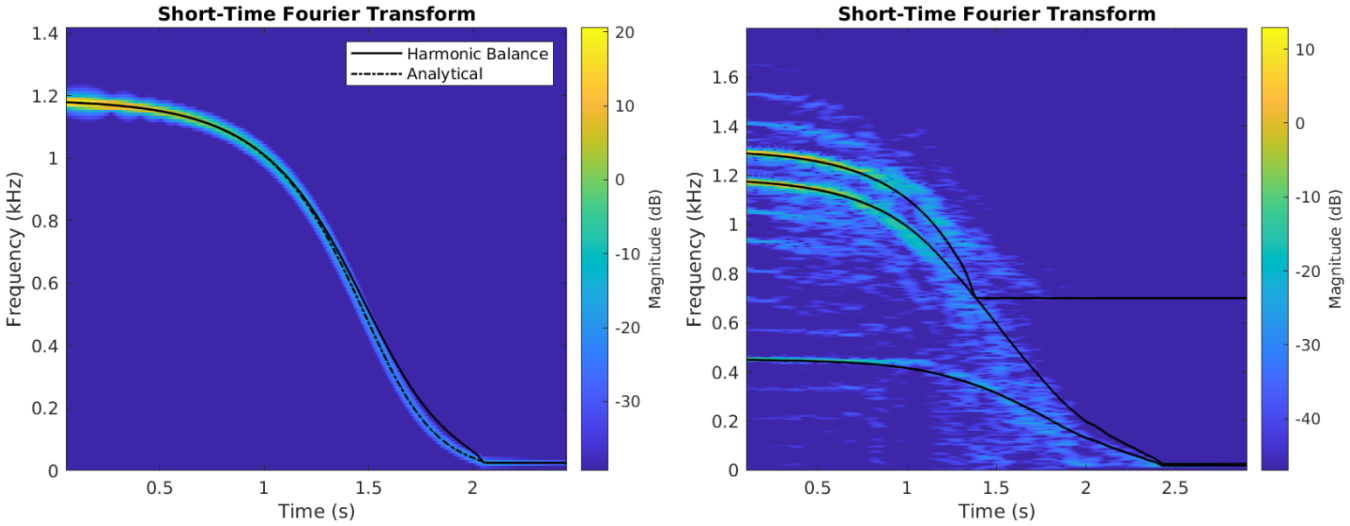

Figure 3. Ringdown response to (left) antisymmetric initial conditions and (right) asymmetric initial conditions.

Exploring the unusual structures apparent in Fig. 3 further, consider the *symmetric* initial conditions $\boldsymbol{x}(0) = [0\ 0\ 0]^T$ and $\dot{\boldsymbol{x}}(0) = [0\ 200\ 0\ \text{m/s}]^{\text{T}}$. Because the initial conditions are symmetric, the response should be as well. However, as shown in Figure 4, the symmetry is broken (by an amount equal to the solver tolerance) at $t \approx 0.8$ s, which roughly corresponds to the loss of coherence in the spectrogram.

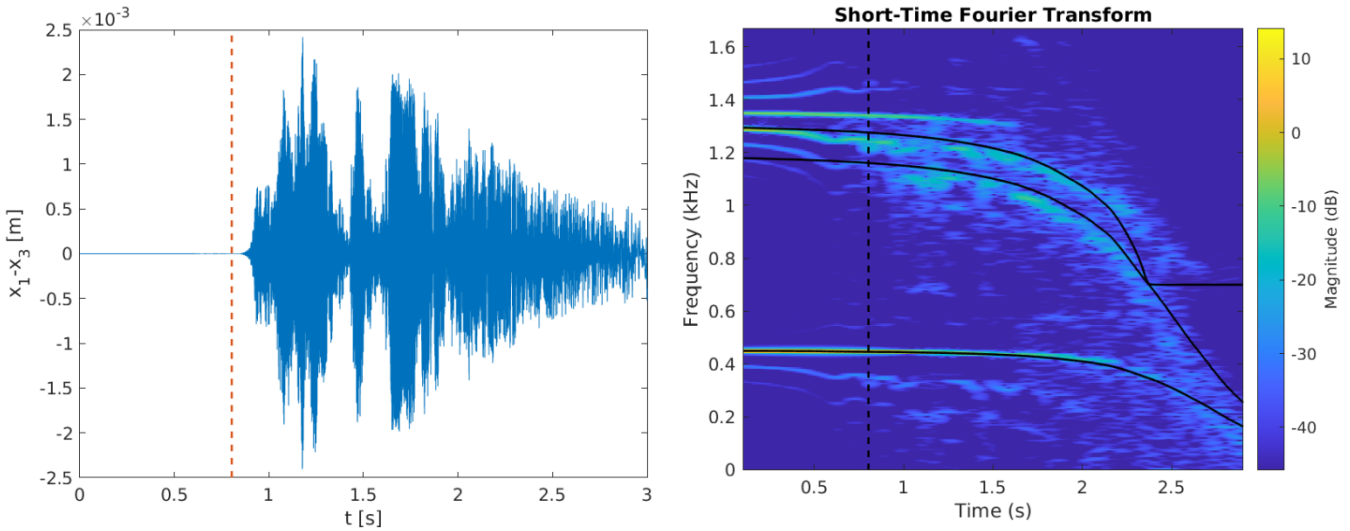

Figure 4. Spontaneous numerical symmetry breaking. The dashed vertical lines indicate the time at which the left-right symmetry is broken by more than the solver tolerance.

3.3 Discussion of Results

In the previous section it was demonstrated that, even using a single-harmonic approximation, the nonlinear normal modes obtained by harmonic balance are successful at predicting the evolution of the most dominant frequency content as the lightly damped system rings down. This was observed for both the case in which the system was initiated along NNM 2, as well as in which the structure responds to an asymmetric initial velocity meant to imitate a shock-type loading. Both cases produced initial responses at high energy levels, thus revealing how the dynamics evolve as light viscous damping forces dissipate energy.

It is evident that modeling a bearing-and-shaft assembly with clearances is challenging to linearize, and such approximations will miss potentially important frequency content that could amplify the response of the system. If the initial conditions are initiated at lower energy levels, the spectra of the response could begin at a different point along NNM backbones and thus produce different dynamics.

Observing Fig. 3 (right) carefully, one can see that much of the "cloudiness" in the spectrogram is absent prior to $t \approx 0.2$ s. Indeed, it seems likely that the complicated structures in the spectrogram are numerical artifacts caused by the accumulation of round-off errors, which appear to generate broadband response. This phenomenon appears to be essentially independent of the integration scheme used, and even occurs if one solves the piecewise linear system analytically and evaluates the resulting expressions numerically.

The time at which this occurs varies depending on the scheme and initial conditions, but attempts have been unsuccessful at delaying it to the point where the entire ringdown can be observed clearly. Figure 4 suggests that the onset of broadband frequency content is somehow associated with the numerical breaking of symmetry. However, symmetry breaking need not occur for this to arise, as suggested by Fig. 3, which displays the unusual behavior despite fact that the response is asymmetric from the outset. The phenomena observed here may be related to numerically induced chaos, which has been studied previously [9, 10].

4. Experimental Setup and Results

A simplified experimental apparatus was developed to demonstrate the effect of contact nonlinearity and validate the analytical results. The setup was developed to mimic bearing-and-shaft assemblies. This was done using a beam (referred to as the impact beam) to represent a shaft and impact tips to mimic the contact nonlinearity present within roller bearings. The impact beam and impact tips were mounted within a box tube as shown in Fig. 5. The whole system was suspended in an approximated free-free boundary condition with bungee cords (via a basket hitch around the box tube) to simplify the boundary condition for analysis.

The impact beam was held in-place via the compressive force from the soft suspension springs, which were glued into pockets on the impact beam and nested into pockets in the box tube. Note that the springs were not fastened or adhered to the box tube. The impact tips were mounted to the box tube through a bolt and load cell assembly. The impact gap could be adjusted by threading the bolt in or out of the beam and the impact stiffness could be adjusted by changing the impact tips.

The system could be excited (with shaker or hammer excitation) through the box tube or directly through the impact beam via a hole in the box tube.

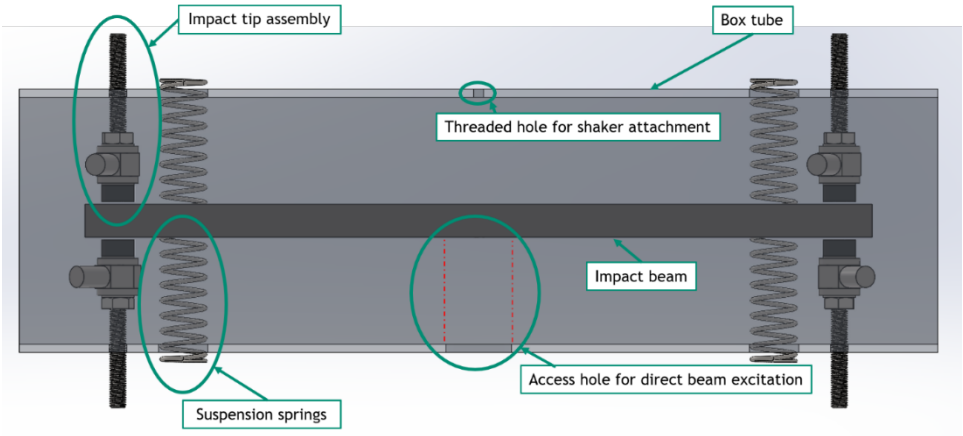

Figure 5. Schematic of simplified shaft/bearing test apparatus.

A corresponding high-fidelity finite element model was also generated, as shown in Fig. 6. The suspension springs were simulated using beam elements along the centerline of the spring. Complex geometries, such as the load cells and fasteners, were simplified while keeping the mass unaffected to preserve the essential dynamics of the system. The model consists of hexahedral elements, except for the suspension springs, with at least three elements through the thickness of the box tube to properly capture bending. Components that are in contact are considered tied except for the impact tip assembly and the beam which use frictional contact to allow for transverse motion while prohibiting penetration.

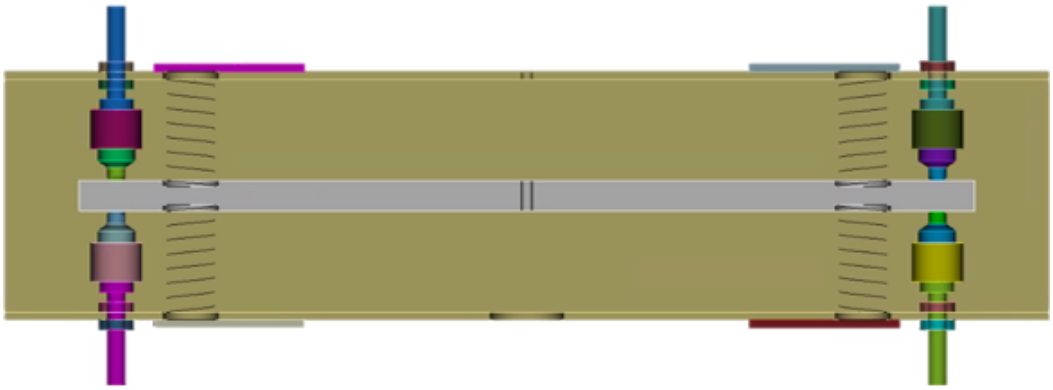

Figure 6. Cross section of finite element model of simplified bearing-and-shaft test apparatus. (Mesh not shown.)

4.1 Instrumentation and Setup

Figure 7 shows the impact beam set-up with six triaxial accelerometers placed along the length to capture the pseudo rigid body modes. The box tube had four triaxial load cells mounted around the centerline, as shown in Fig. 8, to identify the motion of the box tube versus the impact beam. The load cells in the impact tip assembly are also shown in Fig. 8. A linear modal analysis was performed using roving impact hammer test methodology. The impact locations were distributed around the box tube at a variety of locations and directions to excite all six rigid body modes of the impact beam. Additionally, nonlinear transient ringdown data was gathered with impact excitation through the center of the beam. The results from the modal analysis are presented in Section 4.2, while the nonlinear transient ringdown data are presented in Section 4.3.

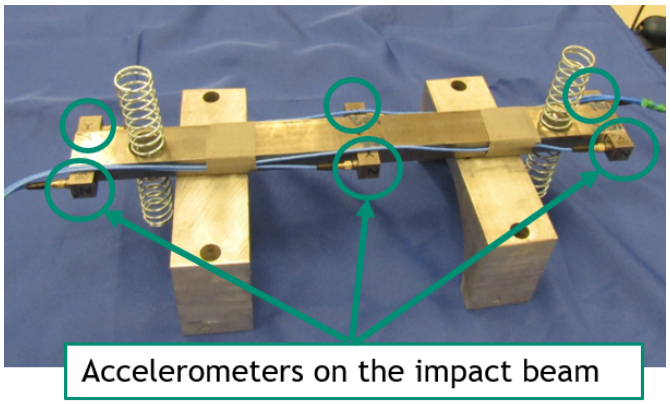

Figure 7. Accelerometer placement on the impact beam.

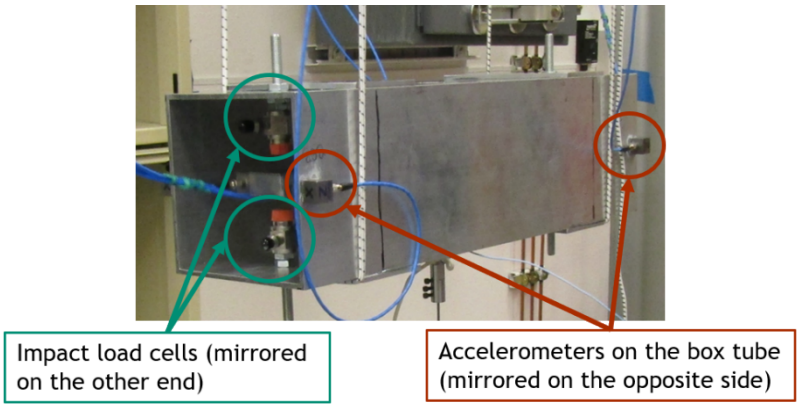

Figure 8. Accelerometer and load cell placement on box frame and impact tip assembly.

4.2 Linear Modal Analysis and Correlation

A correlation was performed comparing the physical test setup in the linear, open gap configuration to the finite element model. Table 2 details a comparison of the natural frequencies, showing a reasonably good correlation in frequency for the pseudo rigid body modes. Modal assurance criterion (MACs) were computed to compare the rigid body modes of the model and those of the test setup. Two MACs were calculated, one for the beam only and another for the whole assembly. Table 3 lists the computed diagonal MAC values, and the MACs are plotted in Fig. 9.

The beam modes are reasonably accurate, with the lowest MAC value at 93.5% for the longitudinal mode and the highest at 99.7% for the roll mode. However, the MAC comparing all DOF from the test assembly to the model show poor MAC values for the longitudinal, lateral, and pitch rigid body modes. This indicates that while the response of the beam itself is well characterized in the model, the response of the assembly as a whole is not well represented for some of the modes of interest. Future work on this system would benefit from further model correlation and updating. However, the response of the beam and the natural frequencies overall were highly accurate between model and test, indicating that the beam response is well characterized.

Table 2. Frequency correlation between test and finite element model for open gap case.

Mode Number	Description	Experimental	Finite Element Model	% Frequency Error
1	Longitudinal	10.92 Hz	10.68 Hz	2.2%
2	Lateral	11.66 Hz	11.24 Hz	3.6%
3	Yaw	15.08 Hz	13.73 Hz	9.0%
4	Bounce	19.94 Hz	18.50 Hz	7.2%
5	Pitch	24.11 Hz	22.65 Hz	6.1%
6	Roll	33.69 Hz	34.72 Hz	-3.1%

Table 3. MAC correlation between test and finite element model for open gap case.

Mode Number	Description	MAC, beam only	MAC, assembly
1	Longitudinal	93.5%	46.0%
2	Lateral	94.1%	46.2%
3	Yaw	98.3%	98.2%
4	Bounce	95.7%	96.1%
5	Pitch	99.4%	60.9%
6	Roll	99.7%	99.1%

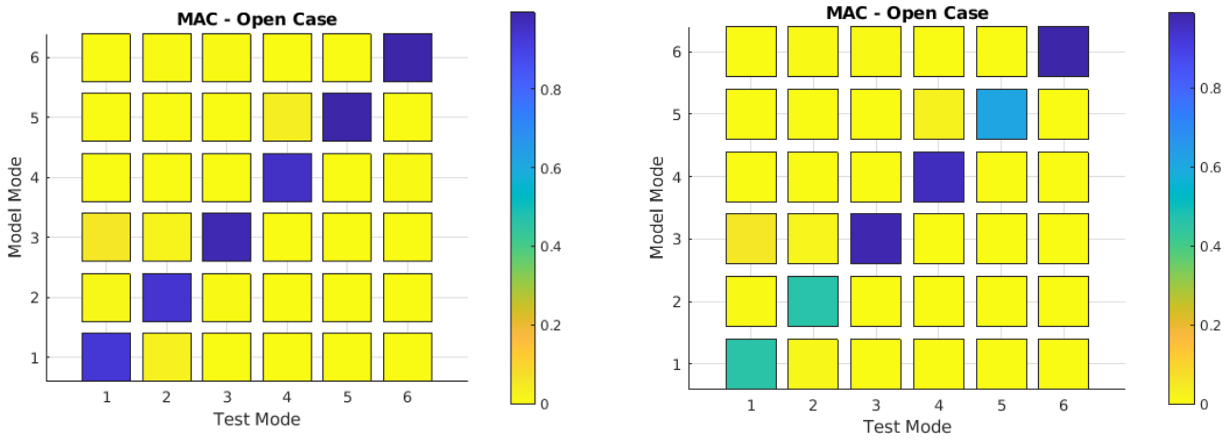

Figure 9. MAC correlation between test and finite element model for open gap case using (left) beam only accelerometers, and (right) all accelerometers.

4.3 Nonlinear Transient Ringdown

Transient ringdown data was collected on the system via an impact at the center of the beam with the following system set-up:

- Impact Tips – white plastic impact hammer tips
- Impact Gap – 0.254 mm

The contact nonlinearity was verified by inspecting the impact tip load cell data, as shown in Fig. 10. A time-frequency analysis was then performed using a short-time Fourier transform. The transient ringdown is clearly seen in the resulting spectrogram that is shown in Fig. 11. This shows the broadband and roll mode vibration decaying into the bounce mode. The ringdown behavior was confirmed to be a physical phenomenon (rather than an artifact of the data processing) through repeated impacts and variations in the processing parameters. While the data here is preliminary, future work will explore the system excited to higher levels to correlate the nonlinear ringdown to predictions from the detailed finite element model.

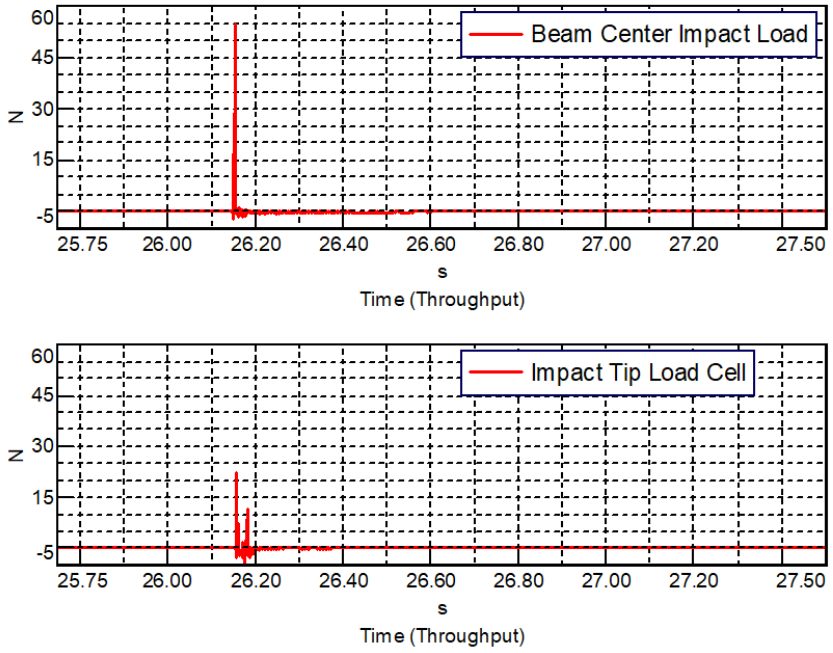

Figure 10. Time history of (top) beam excitation force and (bottom) impact load cell at an impact tip.

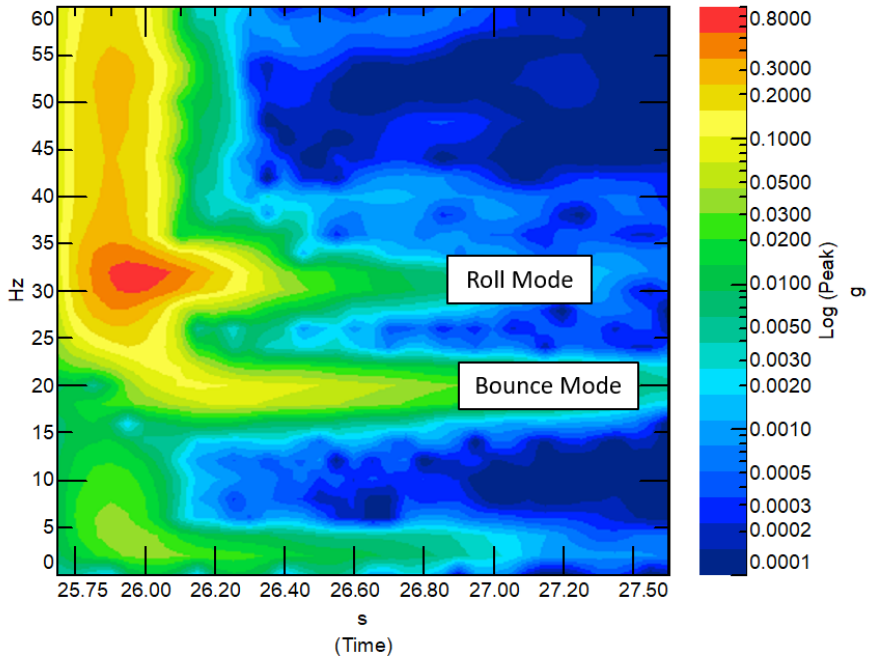

Figure 11. Spectrogram showing the nonlinear transient ringdown acceleration.

5. Conclusion

This paper presented preliminary studies of the contact nonlinearity in bearing-and-shaft systems with a focus on transient free vibration. After recalling the principles of harmonic balance and nonlinear normal modes (NNMs), a simple, three-degree-of-freedom model was formulated to represent a shaft supported between two bearings. Good agreement was found in comparing numerical ringdown solutions to the nonlinear normal modes computed using single-term harmonic balance. An exact analytical solution for NNM 2 was also developed and proved to be accurate. It is evident that the underlying NNMs of the system correlate well to the spectral content of the ringdown for initial conditions both initiated on and off the NNM branch.

The numerical study exposed some of the modeling challenges associated with linearization assumptions needed to model a shaft supported by bearings, in particular when simulating high-amplitude, short-duration mechanical shock. Unusual phenomena that might be related to numerical symmetry breaking and chaos were noted before presenting an experimental apparatus and corresponding finite element model. Some preliminary data from experiment and correlation with a detailed finite element model were shown.

There are several avenues for future work on this subject. A complete understanding of the solution space for the three-degree-of-freedom system is worth obtaining, and significant questions still exist about why spurious symmetry breaking occurs in numerical ringdown solutions and how it is related to the apparent discord in the spectrograms. There is also additional studies required to develop the experimental apparatus further, one example being to reduce the damping in the system so a large number of shaft-bearing contacts occur over the course of a typical experimental run, thus improving the applicability of NNMs to characterize the system.

Acknowledgements

Supported by Laboratory Directed Research and Development program at Sandia National Laboratories, a multimission laboratory managed and operated by National Technology and Engineering Solutions of Sandia LLC, a wholly owned subsidiary of Honeywell International Inc. for the U.S. Department of Energy's National Nuclear Security Administration under contract DE-NA0003525. *This paper describes objective technical results and analysis. Any subjective views or opinions that might be expressed in the paper do not necessarily represent the views of the U.S. Department of Energy or the United States Government.*

References

[1] R. R. J. Craig and A. J. Kurdila, *Fundamentals of Structural Dynamics*, 2nd ed. New York: John Wiley and Sons, 2006.

[2] M. Gzal, A. F. Vakakis, L. A. Bergman, and O. V. Gendelman, "Extreme intermodal energy transfers through vibro-impacts for highly effective and rapid blast mitigation," *Communications in Nonlinear Science and Numerical Simulation,* vol. 103, p. 106012, 2021/12/01/ 2021, doi: https://doi.org/10.1016/j.cnsns.2021.106012.

[3] C. A. Herrera, D. M. McFarland, L. A. Bergman, and A. F. Vakakis, "Methodology for nonlinear quantification of a flexible beam with a local, strong nonlinearity," *Journal of Sound and Vibration,* vol. 388, pp. 298-314, 2017.

[4] G. Kerschen, M. Peeters, J. C. Golinval, and A. F. Vakakis, "Nonlinear normal modes. Part I. A useful framework for the structural dynamicist," *Mechanical Systems and Signal Processing,* vol. 23, no. 1, pp. 170-94, 2009, doi: 10.1016/j.ymssp.2008.04.002.

[5] Z. Feng, M. Liang, and F. Chu, "Recent advances in time–frequency analysis methods for machinery fault diagnosis: A review with application examples," *Mechanical Systems and Signal Processing,* vol. 38, no. 1, pp. 165-205, 2013/07/05/ 2013, doi: https://doi.org/10.1016/j.ymssp.2013.01.017.

[6] M. Krack and J. Gross, *Harmonic Balance for Nonlinear Vibration Problems*, 1st ed. Springer International Publishing, 2019.

[7] T. M. Cameron and J. H. Griffin, "An Alternating Frequency/Time Domain Method for Calculating the Steady-State Response of Nonlinear Dynamic Systems," *Journal of Applied Mechanics,* vol. 56, no. 1, pp. 149-154, 1989, doi: 10.1115/1.3176036.

[8] R. Seydel, *Practical bifurcation and stability analysis*. Springer Science & Business Media, 2009.

[9] M. J. Ablowitz, C. Schober, and B. M. Herbst, "Numerical chaos, roundoff errors, and homoclinic manifolds," *Physical Review Letters,* vol. 71, no. 17, pp. 2683-2686, 10/25/ 1993, doi: 10.1103/PhysRevLett.71.2683.

[10] R. M. Corless, C. Essex, and M. A. H. Nerenberg, "Numerical methods can suppress chaos," *Physics Letters A,* vol. 157, no. 1, pp. 27-36, 1991/07/15/ 1991, doi: https://doi.org/10.1016/0375-9601(91)90404-V.